Paired modes of heterostructure cavities in photonic crystal waveguides with split band edges

Sahand Mahmoodian,[1,*] Andrey A. Sukhorukov,[2] Sangwoo Ha,[2] Andrei V. Lavrinenko,[2,4] Christopher G. Poulton,[3] Kokou B. Dossou,[3] Lindsay C. Botten,[3] Ross C. McPhedran,[1], and C. Martijn de Sterke[1]

[1] *CUDOS and IPOS, School of Physics, University of Sydney, Australia*
[2] *Nonlinear Physics Centre, Research School of Physics and Engineering, Australian National University, Canberra, Australia*
[3] *CUDOS, School of Mathematical Sciences, University of Technology, Sydney, Australia*
[4] *DTU Fotonik, Department of Photonics Engineering, Technical University of Denmark, Lyngby, Denmark*
*sahand@physics.usyd.edu.au

Abstract: We investigate the modes of double heterostructure cavities where the underlying photonic crystal waveguide has been dispersion engineered to have two band-edges inside the Brillouin zone. By deriving and using a perturbative method, we show that these structures possess two modes. For unapodized cavities, the relative detuning of the two modes can be controlled by changing the cavity length, and for particular lengths, a resonant-like effect makes the modes degenerate. For apodized cavities no such resonances exist and the modes are always non-degenerate.

OCIS codes: (140.3948) Microcavity devices; (130.5296) Photonic crystal waveguides; (130.2790) Guided waves; (350.4238) Nanophotonics and photonic crystals; (050.5298) Photonic crystals; (230.5298) Photonic crystals; (160.5298) Photonic crystals.

References and links

1. K. Nozaki, T. Tanabe, A. Shinya, S. Matsuo, T. Sato, H. Taniyama, and M. Notomi, "Sub-femtojoule all-optical switching using a photonic-crystal nanocavity," Nat. Photonics **4**, 477–483 (2010).
2. J. Vučković and Y. Yamamoto, "Photonic crystal microcavities for cavity quantum electrodynamics with a single quantum dot," Appl. Phys. Lett. **82**, 2374–2376 (2003).
3. M. Eichenfield, J. Chan, R. M. Camacho, K. J. Vahala, and O. Painter, "Optomechanical crystals," Nature **462**, 78–82 (2009).
4. O. Painter, R. K. Lee, A. Scherer, A. Yariv, J. D. O'Brien, P. D. Dapkus, and I. Kim, "Two-dimensional photonic band-gap defect mode laser," Science **284**, 1819–1821 (1999).
5. B. S. Song, S. Noda, T. Asano, and Y. Akahane, "Ultra-high-Q photonic double-heterostructure nanocavity," Nat. Mater. **4**, 207–210 (2005).
6. E. Kuramochi, M. Notomi, S. Mitsugi, A. Shinya, T. Tanabe, and T. Watanabe, "Ultrahigh-Q photonic crystal nanocavities realized by the local width modulation of a line defect," Appl. Phys. Lett. **88**, 041112 (2006).
7. Y. Tanaka, T. Asano, and S. Noda, "Design of photonic crystal nanocavity with Q-factor of $\sim 10^9$," J. Lightwave Technol. **26**, 1532–1539 (2008).
8. S. Tomljenovic Hanic, M. J. Steel, C. M. de Sterke, and D. J. Moss, "High-Q cavities in photosensitive photonic crystals," Opt. Lett. **32**, 542–544 (2007).
9. S. Gardin, F. Bordas, X. Letartre, C. Seassal, A. Rahmani, R. Bozio and P. Viktorovitch, "Microlasers based on effective index confined slow light modes in photonic crystal waveguides," Opt. Express **16**, 6331–6339 (2008).
10. T. Asano, B. S. Song, Y. Akahane, and S. Noda, "Ultrahigh-Q nanocavities in two-dimensional photonic crystal slabs," IEEE J. Sel. Top. Quantum Electron. **12**, 1123–1134 (2006).

#135404 - $15.00 USD Received 21 Sep 2010; revised 18 Nov 2010; accepted 20 Nov 2010; published 23 Nov 2010

11. D. Englund, I. Fushman, and J. Vučković, "General recipe for designing photonic crystal cavities," Opt. Express **13,** 5961–5975 (2005).
12. M. Ibanescu, S. G. Johnson, D. Roundy, Y. Fink, and J. D. Joannopoulos, "Microcavity confinement based on an anomalous zero group-velocity waveguide mode," Opt. Lett. **30,** 552–554 (2005).
13. A. Figotin and I. Vitebskiy, "Slow-wave resonance in periodic stacks of anisotropic layers," Phys. Rev. A **76,** 053839 (2007).
14. A. A. Chabanov, "Strongly resonant transmission of electromagnetic radiation in periodic anisotropic layered media," Phys. Rev. A **77,** 033811 (2008).
15. K. Y. Jung and F. L. Teixeira, "Numerical study of photonic crystals with a split band edge: Polarization dependence and sensitivity analysis," Phys. Rev. A **78,** 043826 (2008).
16. S. Ha, A. A. Sukhorukov, A. V. Lavrinenko, and Yu. S. Kivshar, "Cavity mode control in side-coupled periodic waveguides: theory and experiment," Photonics Nanostruct.: Fundam. Appl. **8,** 310–317 (2010).
17. S. Mahmoodian, C. G. Poulton, K. B. Dossou, R. C. McPhedran, L. C. Botten, and C. M. de Sterke, "Modes of Shallow Photonic Crystal Waveguides: Semi-Analytic Treatment," Opt. Express **17,** 19629–19643 (2009).
18. J. M. Luttinger and W. Kohn, "Motion of electrons and holes in perturbed periodic fields," Phys. Rev. **97,** 869–883 (1955).
19. J. D. Joannopoulos, R. D. Meade, and J. N. Winn, *Photonic Crystals: Molding the Flow of Light* (Princeton University Press, Princeton, 1995).
20. P. St. J. Russell, T. A. Birks, and F. D. Lloyd Lucas, "Photonic Bloch waves and photonic band gaps," in *Confined Electrons and Photons*, E. Burstein and C. Weisbuch, eds., (1995), pp. 585–633.
21. S. W. Ha, A. A. Sukhorukov, K. B. Dossou, L. C. Botten, A. V. Lavrinenko, D. N. Chigrin, and Yu. S. Kivshar, "Dispersionless tunneling of slow light in antisymmetric photonic crystal couplers," Opt. Express **16,** 1104–1114 (2008).
22. M. W. Lee, C. Grillet, S. Tomljenovic Hanic, E. C. Magi, D. J. Moss, B. J. Eggleton, X. Gai, S. Madden, D. Y. Choi, D. A. P. Bulla, and B. Luther-Davies, "Photowritten high-Q cavities in two-dimensional chalcogenide glass photonic crystals," Opt. Lett. **34,** 3671–3673 (2009).

1. Introduction

Optical cavities that confine light over many optical cycles are much studied devices in modern photonics. Such cavities have been realised by using photonic crystals (PC) where an optical bandgap is used to confine light. The use of such PC based cavities has been reported in a wide range of experiments including all optical switching [1], cavity quantum electrodynamics [2], optomechanical interactions [3], and such structures have also been used to construct low threshold lasers [4]. In all cases, the purpose of the cavity is to strengthen the interaction of light with matter. This means that it is often desirable to maximize the quality factor of the cavity while minimizing its modal volume.

A type of PC cavity with a very high quality factor to modal volume ratio is the double heterostructure cavity (DHC). DHCs have been shown to achieve experimental quality factors of $\sim 10^6$ [5, 6] and theoretical quality factors of greater than 10^8 [7] while maintaining a modal volume of $\sim (\lambda_0/n)^3$. As shown in Fig. 1(a), DHCs are constructed by weakly perturbing a photonic crystal waveguide (PCW). This can be done, for example, by changing the period of the PCW [5], shifting the position of cylinders [6], altering the refractive index of the background [8] or even by adding a superstrate [9]. The dispersion curve associated with the PCW in the perturbed region is offset from that of the unperturbed region. This creates a modegap, where modes bound to the perturbed region can exist. Recently, much effort has gone into tailoring the nature of the perturbation to minimize coupling into unbound states and maximising the quality factor [7, 10, 11]. This is achieved by constructing a perturbation that "gently" confines light in the direction along the PCW, reducing out-of-plane losses and hence increasing its quality factor [10, 11].

On the other hand, it was found that the existence and characteristics of cavity modes are fundamentally modified if optical resonators are based on waveguides whose dispersion features 'split band-edges' (SBE), which appear inside the Brillouin zone (BZ). Examples of such resonators include sections of omniguide fibers [12], periodic structures with anisotropic layers [13–15], and side-coupled periodic waveguides [16]. In particular, it was shown that there

#135404 - $15.00 USD Received 21 Sep 2010; revised 18 Nov 2010; accepted 20 Nov 2010; published 23 Nov 2010

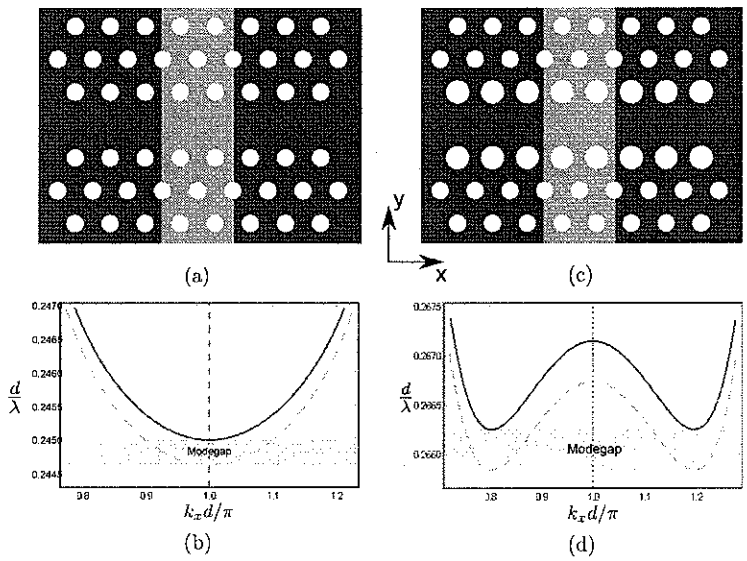

Fig. 1. Schematic of DHCs and their dispersion curves. (a) DHC based on a W1 waveguide. The highlighted region indicates the underlying PCW being perturbed to create a cavity. (b) Dispersion curve of the W1 PCW. Broken cyan curve shows the dispersion curve of a PCW with the background index changed to $n_b = 3.005$. Green highlighting shows the mode gap. Vertical dashed line indicates BZ edge. (c) A DHC based on a PCW where the holes adjacent to the waveguide have had their radius increased to engineer the dispersion of the band minimum. (d) Dispersion curve of dispersion engineered PCW. The two band minima are at $k_x d/\pi = \pm 0.8034$ (a reciprocal lattice vector is added in figure).

appear two pairs of forward and backward propagating waves arbitrarily close to split band edges, and nontrivial coupling between all four waves can give rise to a pair of cavity modes with nontrivial tuning properties [16].

In this paper, we show that the combination of the two concepts, double heterostructure cavities and split band-edges, opens new possibilities for controlling the cavity modes in PCs. Whereas a conventional W1 PCW has dispersion with a single band-edge appearing at the BZ edge [Figs. 1(a) and 1(b)], we can perform dispersion engineering leading to SBE by altering the radius of the holes adjacent to the PCW [Figs. 1(c) and 1(d)]. Previous analysis [10] has shown that a DHC mode is essentially made up of an envelope function that modulates the band-edge Bloch mode of the underlying PCW. Here, using perturbation theory, we show that when there are two inequivalent band-edge states inside the BZ due to SBE, the DHC mode is made up of a superposition of the two band-edge Bloch modes, each modulated by its own envelope function. As there are two band-edge Bloch states, the DHC has two bound modes. The nature of these two modes depends on how the perturbation that creates the DHC couples the band-edge Bloch states. We find that for unapodized perturbations the coupling of the band-edge Bloch states can be altered by changing the length of the cavity. This changes the relative detuning of the two DHC modes and for particular lengths makes them degenerate. Using our theory, we show that for apodized cavities these degeneracies do not exist and the detuning simply decreases with increasing cavity length.

#135404 - $15.00 USD Received 21 Sep 2010; revised 18 Nov 2010; accepted 20 Nov 2010; published 23 Nov 2010

2. Formulation of theory

We begin by outlining our theory which we use to analyse the physics governing the underlying behaviour of the DHC modes. As in our previous work on PCWs [17], our approach is based on the effective mass theory by Luttinger and Kohn [18], adapted to PCs. For simplicity, we analyse the problem for a two dimensional PC. Generalising the theory to PC slab structures is straightforward, but is not within the scope of this paper as it does not affect the physics we discuss. In this geometry, we take the unperturbed structure as a PCW that is periodic in the x-direction (see Fig. 1) and is dispersion engineered in a fashion such that the minima of its dispersion relation are not at the BZ edge or centre [Fig. 1(d)]. Throughout this paper we look at H_z polarised modes of a PCW with a background index $n_b = 3.0$, air holes of radius $0.3d$, where d is the period, and the radius of the holes adjacent to the waveguide are changed to $0.4d$. The equation governing the modes of the PCW is

$$\nabla \times \nabla \times \mathbf{E}_{k_x}(\mathbf{r}) = \frac{\varepsilon(\mathbf{r})\omega_{k_x}^2}{c^2}\mathbf{E}_{k_x}(\mathbf{r}), \tag{1}$$

where $\varepsilon(\mathbf{r})$ is the permittivity of the PCW and the subscript k_x indicates the dependence on the Bloch wavevector. The cavity mode then satisfies

$$\nabla \times \nabla \times \mathbf{E}(\mathbf{r}) = \frac{[\varepsilon(\mathbf{r}) + \delta\varepsilon(\mathbf{r})]\omega^2}{c^2}\mathbf{E}(\mathbf{r}), \tag{2}$$

where we have constructed the cavity by adding the perturbation $\delta\varepsilon(\mathbf{r})$ as shown in Fig. 1. We choose to expand the cavity modes using the Bloch basis set, that is, the modes of the PCW. Here we can choose our basis set such that we can use the wavevector k_x, spanning all reciprocal space, to index our modes. The expansion takes the form

$$\mathbf{E}(\mathbf{r}) = \int_{-\infty}^{\infty} dk_x C(k_x)\mathbf{E}_{k_x}(\mathbf{r}). \tag{3}$$

Substituting Eq. (3) in Eq. (2), using Eq. (1) and taking the inner product with $\mathbf{E}^*_{k'_x}(\mathbf{r})$, we obtain the expression in reciprocal space

$$C(k'_x)[\omega_{k'_x}^2 - \omega^2]M = \omega^2 \int_{-\infty}^{\infty} dk_x C(k_x) \int_{\mathbb{R}^2} d\mathbf{r}\, \delta\varepsilon(\mathbf{r})\mathbf{E}^*_{k'_x}(\mathbf{r}) \cdot \mathbf{E}_{k_x}(\mathbf{r}), \tag{4}$$

where the normalisation condition $\int_{\mathbb{R}^2} \varepsilon(\mathbf{r})\mathbf{E}^*_{k'_x}(\mathbf{r}) \cdot \mathbf{E}_{k_x}(\mathbf{r})d\mathbf{r} = M\delta(k'_x - k_x)$ has been used.

We now need to make further approximations if we wish to proceed analytically. DHCs are typically created by weakly perturbing a PCW, and consequently their modes are weakly bound along the x-direction. Thus the typical width of a DHC mode is larger than a period of the PCW. $C(k_x)$ is then expected to be narrow in reciprocal space. Since there are two inequivalent band minima, $C(k_x)$ is then composed of two narrow peaks centred on each minimum. We can thus write $C(k_x) = F_1(k_x - k_L^{(1)}) + F_2(k_x - k_L^{(2)})$, where $k_L^{(1)}$ and $k_L^{(2)}$ are the Bloch wavevectors of the two band minima. We note that according to the general symmetry properties of Bloch modes in dielectric PCs [19–21],

$$k_L^{(2)} = -k_L^{(1)}, \quad \omega_{k_x} = \omega_{-k_x}, \quad \mathbf{E}_{k_x}(\mathbf{r}) = \mathbf{E}^*_{-k_x}(\mathbf{r}). \tag{5}$$

Provided that the separation between $k_L^{(1)}$ and $k_L^{(2)}$ is large compared to their widths we can rewrite Eq. (4) as two equations, one where k'_x has values where the function $F_1(k_x - k_L^{(1)})$ is

#135404 - $15.00 USD Received 21 Sep 2010, revised 18 Nov 2010, accepted 20 Nov 2010; published 23 Nov 2010

dominant and another where $F_2(k_x - k_L^{(2)})$ is dominant. The first of the two equations is

$$F_1(k'_x - k_L^{(1)})(\omega_{k'_x}^2 - \omega^2) = \omega^2 \int_{-\infty}^{\infty} dk_x [F_1(k_x - k_L^{(1)}) + F_2(k_x - k_L^{(2)})] \int_{\mathbb{R}^2} d\mathbf{r}\, \delta\varepsilon(\mathbf{r}) \mathbf{E}^*_{k'_x}(\mathbf{r}) \cdot \mathbf{E}_{k_x}(\mathbf{r}). \tag{6}$$

We now multiply by $\exp[i(k'_x - k_L^{(1)})x']$ and integrate over k'_x. On the left hand side this gives

$$M(\omega^2_{-i\frac{d}{dx'}} - \omega^2) f_1(x') \tag{7}$$

where $f_1(x) = \int_{\infty}^{\infty} F_1(k_x - k_L^{(1)}) e^{i(k_x - k_L^{(1)})x} dk_x$ is an envelope function. The operator, $\omega^2_{-id/dx}$ denotes an expansion about the band minimum in powers of $-id/dx$ and arises as a result of inverse Fourier transforming with respect to k'_x. It is given by $\omega^2_{-id/dx} \sim \omega_L^2 - (\omega_L/D_L)d^2/dx^2$, where ω_L is the frequency of the band-edge and D_L is the curvature of the band-edge. We choose to keep only the leading order derivative as the band-edge is quadratic to first order and the envelope function along x is slowly varying compared to the period of the PCW. We now turn to the RHS of Eq. (6). Since F_1 and F_2 are narrow functions, the main Bloch mode contribution is from the Bloch mode corresponding to the Bloch wavevector upon which the minimum is centred, that is, modes corresponding to the Bloch wavevectors $k_L^{(1)}$ and $k_L^{(2)}$ respectively. We thus write $\mathbf{E}_{k_x}(\mathbf{r}) \sim \mathbf{E}_{k_L^{(j)}}(\mathbf{r}) e^{i(k_x - k_L^{(j)})x}$ where j denotes either 1 or 2. After some manipulation, the final equation is

$$\hat{L} f_1(x) = \frac{2\pi\omega^2}{M} [f_1(x)\delta\mathscr{E}_{11} + f_2(x)\delta\mathscr{E}_{12}], \tag{8}$$

where $f_1(x)$ and $f_2(x)$ are envelope functions and

$$\hat{L} = (\omega^2 - \omega^2_{-i\frac{d}{dx}}), \quad \delta\mathscr{E}_{jm} = \int_{-\infty}^{\infty} dy\, \delta\varepsilon(\mathbf{r})\, \mathbf{E}^*_{k_L^{(j)}}(\mathbf{r}) \cdot \mathbf{E}_{k_L^{(m)}}(\mathbf{r}). \tag{9}$$

Due to the symmetry relations formulated in Eq. (5), $\delta\mathscr{E}_{11} = \delta\mathscr{E}_{22}$ and $\delta\mathscr{E}_{12} = \delta\mathscr{E}^*_{21}$. Carrying out the same process as above for the second equation we write the two equations in matrix form giving

$$\begin{bmatrix} \hat{L} + \frac{\omega^2 d}{\mathscr{E}}\delta\mathscr{E}_{11}(x) & \frac{\omega^2 d}{\mathscr{E}}\delta\mathscr{E}_{12}(x) \\ \frac{\omega^2 d}{\mathscr{E}}\delta\mathscr{E}^*_{12}(x) & \hat{L} + \frac{\omega^2 d}{\mathscr{E}}\delta\mathscr{E}_{11}(x) \end{bmatrix} \begin{bmatrix} f_1(x) \\ f_2(x) \end{bmatrix} = \begin{bmatrix} 0 \\ 0 \end{bmatrix}, \tag{10}$$

where we have recast the normalisation parameter M in terms of that over a unit cell, that is, $M = (2\pi/d)\mathscr{E}$ with $\mathscr{E} = \int_{\text{cell}} dx \int_{-\infty}^{\infty} dy\, \varepsilon(\mathbf{r}) ||\mathbf{E}(\mathbf{r})||^2$. We note that the diagonal terms are equivalent and the off-diagonal terms are each other's complex conjugates, as a consequence of symmetry relations in Eq. (5). Thus, when computing the frequency of the DHC modes the magnitude of the diagonal terms determine how deeply the frequency of the modes moves into the modegap, while the off-diagonal terms determine the relative frequency detuning of the two states. The states will then become degenerate if the contribution of the off-diagonal terms vanishes.

Finally, from Eq. (3) the cavity mode is given by

$$\mathbf{E}(\mathbf{r}) = f_1(x)\mathbf{E}_{k_L^{(1)}}(\mathbf{r}) + f_2(x)\mathbf{E}_{k_L^{(2)}}(\mathbf{r}), \tag{11}$$

which implies that the mode is composed of a superposition of band-edge Bloch modes each modulated by an envelope function given by solving Eq. (10). By using the symmetry relations

#135404 - $15.00 USD Received 21 Sep 2010; revised 18 Nov 2010; accepted 20 Nov 2010; published 23 Nov 2010

in Eq. (5), we can rewrite Eq. (11) as

$$\mathbf{E}(\mathbf{r}) = f_R(x)\mathrm{Re}\left[\mathbf{E}_{k_L^{(1)}}(\mathbf{r})\right] + f_I(x)\mathrm{Im}\left[\mathbf{E}_{k_L^{(1)}}(\mathbf{r})\right], \tag{12}$$

where $f_R = f_1 + f_2$ and $f_I = if_1 - if_2$. Accordingly, the eigenmode of Eq. (10) can be reformulated for the real envelope functions $f_R(x)$ and $f_I(x)$,

$$\begin{bmatrix} \hat{L} + \frac{\omega^2 d}{c^2}\left[\delta\mathscr{E}_{11}(x) + \mathrm{Re}\left(\delta\mathscr{E}_{12}(x)\right)\right] & -\frac{\omega^2 d}{c^2}\mathrm{Im}\left[\delta\mathscr{E}_{12}(x)\right] \\ -\frac{\omega^2 d}{c^2}\mathrm{Im}\left[\delta\mathscr{E}_{12}(x)\right] & \hat{L} + \frac{\omega^2 d}{c^2}\left[\delta\mathscr{E}_{11}(x) - \mathrm{Re}\left(\delta\mathscr{E}_{12}(x)\right)\right] \end{bmatrix} \begin{bmatrix} f_R(x) \\ f_I(x) \end{bmatrix} = \begin{bmatrix} 0 \\ 0 \end{bmatrix}. \tag{13}$$

We now can see from Eqs. (12) and (13) that the profiles of cavity modes are real-valued (up to a constant overall phase), being a superposition of real and imaginary parts of the complex Bloch waves with the corresponding envelope functions. Although the phase of a Bloch function can be chosen freely, leading to changes in its real and imaginary parts, the final mode profile does not depend on the overall phase of the Bloch wave.

3. Results and Discussion

We now use our theory to compute the DHC modes. We examine unapodized cavities where we create the DHC by altering the refractive index of the background material by $\Delta n = 0.005$, as well as apodized cavities where the index of the background is altered according to a Gaussian profile with a maximum index change of $\Delta n = 0.005$. Creating the cavity in this way is similar to the photosensitive cavities previously investigated numerically in [8] and experimentally in [22]. Figures 2(a) and 2(d) show the frequency of the DHC modes as a function of the length of the cavity for unapodized and Gaussian cavities respectively. Here, the numerical calculations were carried out using the finite element package COMSOL. The existence of two modes is a result of the fact that there are two band minima. We highlight the intertwining of the two lines in Fig. 2(a). The difference in frequency of the two modes is shown in Figs. 2(b) and 2(e). This frequency splitting is associated with the off-diagonal terms in Eq. (10). There is a small discrepancy between the numerics and our theory for the splitting as result of using a single band-edge mode at each minimum and assuming weak coupling between the two minima. These assumptions lead to a slight difference between numerics and theory in the k-space distribution of the field, in turn leading to a slight shift in the positions of the zero-crossings in Fig. 2(b). To correct this discrepancy a higher order theory would be necessary. As shown in Figs. 2(c) and 2(f), the average frequency of the two modes is in excellent agreement with the numerics, which indicates that the diagonal terms in Eq. (10) accurately describe how deep the modes move into the bandgap. Importantly, our theory highlights the key difference between the apodized and unapodized cavities, that is, the unapodized cavities have modes whose detuning oscillates with width, while the apodized cavity's modes have a detuning which decreases with cavity length.

Figures 3(a) and 3(b) show the modes of the DHC with a length of $9d$ computed with our perturbation theory. Here, the odd mode is now the fundamental mode as, from Fig. 2(a), it is evident that the modes have crossed. Figure 3(c) shows a comparison between a full numerical calculation of the fields and our perturbation theory. The good agreement indicates that the theory correctly computes both the decay rate of the envelope functions as well as their phases. From these figures it is clear that the perturbation theory contains the underlying physics governing the behaviour of these modes. The theory thus has the potential to be used as a first-principles guide to designing such structures.

We now analyse the modes of the unapodized cavity. As shown in Fig. 2(a) both the numerical solutions and the perturbation theory predict crossings of the two modes at periodic

#135404 - $15.00 USD Received 21 Sep 2010, revised 18 Nov 2010, accepted 20 Nov 2010, published 23 Nov 2010

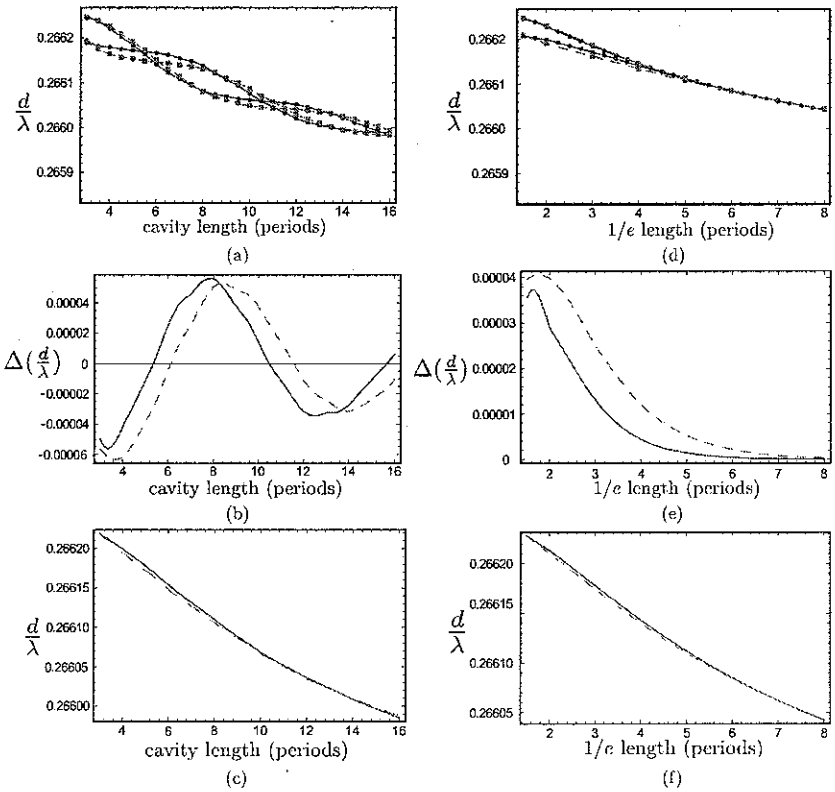

Fig. 2. (a) Frequency of DHC modes versus cavity length for unapodized cavity in PCW with background index $n_b = 3.0$, air hole radius $0.3d$, where d is the period, and radius of holes adjacent to the waveguide are changed to $0.4d$. The background index has been altered to $n_b = 3.005$ to create the cavity. Broken red line corresponds to modes calculated using a fully numerical computation (COMSOL). The blue line corresponds to modes calculated using our perturbation theory. Top of figure corresponds to the band-edge frequency, $d/\lambda = 0.26626$, while the bottom is the frequency of the edge of the modegap, $d/\lambda = 0.26584$. (b) The detuning of the frequency of the two modes in (a). (c) Average of frequencies of the two modes in (a). (d)-(f) Same as (a)-(c) but for the Gaussian cavity with a maximum background index of $n_b = 3.005$.

intervals, meaning that we expect the fundamental mode to alternate from being even to odd with respect to the cavity centre. From Eq. (10) it is apparent that this behaviour is associated with the contribution of the off-diagonal terms. When these terms are large, the difference in frequency of the two modes is large, and when their contribution vanishes, the equations decouple and the modes are degenerate. Here, the $\delta\mathscr{E}_{ij}^{\circ}(x)$ terms depend on x and do not completely vanish unless the perturbation is zero. At the degenerate points however, they evidently have no net contribution to the frequency of the DHC modes. From the symmetry relations in Eq. (5), it is easy to see that the off-diagonal terms are oscillating complex valued functions. When these terms are such that they average to zero along the length of the cavity, the contributions of the off-diagonal terms vanish and the modes become degenerate.

Figure 2(b) shows the frequency of the modes for the apodized cavity. Here, the dependence

#135404 - $15.00 USD Received 21 Sep 2010; revised 18 Nov 2010; accepted 20 Nov 2010; published 23 Nov 2010

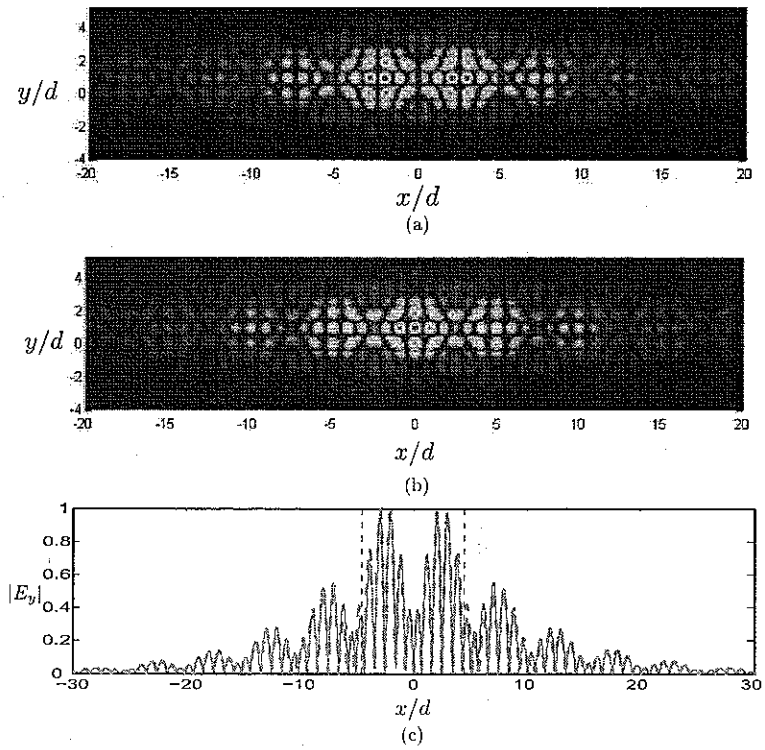

Fig. 3. Normalised amplitudes (arbitrary units) of $|E_y|$ for the DHC modes where the DHC has a length of $9d$ and is centred on $x/d = 0$. (a) $|E_y|$ for the fundamental mode with frequency $d/\lambda = 0.26607$ computed using perturbation theory. (b) $|E_y|$ for the higher order mode with frequency $d/\lambda = 0.26611$ computed using perturbation theory. (c) Cross section of (a) taken along the centre of the PCW (blue curve), but with an added comparison to fully numerical calculations of the fields using a finite element method (COMSOL) (broken red curve). Broken vertical lines indicate the edges of the cavity.

of the frequency of the modes on the length of the cavity is different to that of the unapodized cavity. This difference between the apodized and unapodized cavities is best explained in terms of the envelope functions in reciprocal space. Recall that the functions $F_1(k_x - k_L^{(1)})$ and $F_2(k_x - k_L^{(2)})$ are the FTs of the envelope functions. As the envelope of the DHC mode is slowly varying, these functions are narrow in comparison to their separation in reciprocal space and thus couple weakly. In order to illustrate how the band extrema couple in reciprocal space, we solve Eq. (10) with the coupling terms artificially set to zero. This gives us the shape of $F_1(k_x - k_L^{(1)})$ and $F_2(k_x - k_L^{(2)})$ in the absence of coupling. This is shown for the unapodized cavity in Fig. 4(a). The sidelobes of the maximum centred on the origin are associated with the reflections at the abrupt sidewalls of the cavity [10]. The blue curve is for a cavity with length $10.5d$ and has a zero at $k_x d - k_L^{(1)} d \sim 1.2$. This zero coincides very closely to the centre of the equivalent peak for $F_2(k_x - k_L^{(2)})$ and thus the frequencies of the two modes of a DHC with length $10.5d$ are almost degenerate [c.f. Fig. 2(a)]. The broken green line in Fig. 4(a) is for a cavity with length

#135404 - $15.00 USD Received 21 Sep 2010; revised 18 Nov 2010; accepted 20 Nov 2010; published 23 Nov 2010

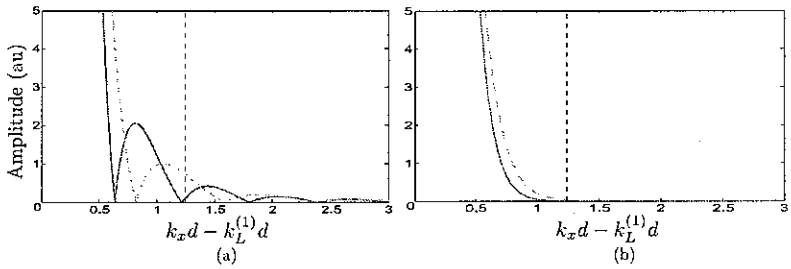

Fig. 4. Sidelobes of $F_1(k_x - k_L^{(1)})$ (arbitrary units) in the absence of coupling. (a) Broken green curve is for an unapodized cavity of length $8d$. The blue curve is for an unapodized cavity with length $10.5d$, i.e. near a point where the modes become degenerate. Although not shown, $F_2(k_x - k_L^{(1)})$ has the same shape as $F_1(k_x - k_L^{(1)})$, but is centred on $k_x = k_L^{(2)}$ indicated by the vertical dashed line. (b) Same as (a) but for a Gaussian cavity. The broken green curve is for a cavity with a $1/e$ length of $4d$, while the blue curve is for a cavity with a $1/e$ length of $5.25d$.

$8d$. Its sidelobes do not have a zero near $k_x = k_L^{(2)}$ and thus its modes are strongly coupled. We thus deduce that when one of the sidelobes of $F_1(k_x - k_L^{(1)})$ coincides with the point where $F_2(k_x - k_L^{(2)})$ is centred, it decouples the contribution from the two band extrema and the modes become degenerate. These sidelobes lead to the intersections of the frequency of the DHC modes as a function of the cavity length shown in Fig. 2(a). The function $F_1(k_x - k_L^{(1)})$ in the absence of coupling for a Gaussian cavity is shown in Fig. 4(b). Here, the reflections at the edges of the cavity are "gentle" and as a result such sidelobes do not exist in reciprocal space. The behaviour of the frequency of DHC modes for apodized cavities is then simple: as the cavity length increases the envelope becomes wider in space and more confined in reciprocal space and hence the coupling between the two band extrema decreases. This agrees with the behaviour shown in Fig. 2(b).

Although we used a two-dimensional model to analyze the modes of split band DHCs, we expect to observe the same behavior for such modes in PC slab structures. In fact, our theoretical model can still be used in PC slab structures with minor modifications. A three-dimensional derivation ends up only differing via the integral in Eq. (9), which also contains an integration over the out-of-plane coordinate.

4. Conclusion

In conclusion, we have suggested and demonstrated new approaches for flexible control of cavity modes in double-heterostructure photonic-crystal cavities. We have shown that cavities created in dispersion engineered photonic crystal waveguides featuring split band edges inside the Brillouin zone generally support a pair of cavity modes. The mode detuning depends non-trivially on the length and shape (apodized or unapodized) of the cavity region, offering possibilities to either increase or fully cancel the mode detuning. We also anticipate that these results may lead to advances in realization of tailored nonlinear light-matter interactions based on the paired cavity modes.

Acknowledgements

The support of the Australian Research Council through its Centres of Excellence and Discovery Programs is acknowledged.

#135404 - $15.00 USD Received 21 Sep 2010, revised 18 Nov 2010, accepted 20 Nov 2010, published 23 Nov 2010